

Higher-order topological insulators and semimetals in generalized Aubry-André-Harper models

Qi-Bo Zeng^{1,*}, Yan-Bin Yang^{1,*} and Yong Xu^{1,2†}

¹Center for Quantum Information, IIIS, Tsinghua University, Beijing 100084, People's Republic of China and
²Shanghai Qi Zhi Institute, Shanghai 200030, People's Republic of China

Higher-order topological phases of matter have been extensively studied in various areas of physics. While the Aubry-André-Harper model provides a paradigmatic example to study topological phases, it has not been explored whether a generalized Aubry-André-Harper model can exhibit a higher-order topological phenomenon. Here, we construct a two-dimensional higher-order topological insulator with chiral symmetry based on the Aubry-André-Harper model. We find the coexistence of zero-energy and nonzero energy corner-localized modes. The former is protected by the quantized quadrupole moment, while the latter by the first Chern number of the Wannier band. The nonzero-energy mode can also be viewed as the consequence of a Chern insulator localized on a surface. More interestingly, the non-zero energy corner mode can lie in the continuum of extended bulk states and form a bound state in the continuum of higher-order topological systems. We finally propose an experimental scheme to realize our model in electric circuits. Our study opens a door to further study higher-order topological phases based on the Aubry-André-Harper model.

Recently, topological phases of matter have made substantial progress due to the discovery of higher-order topological insulators (HOTIs). The HOTIs are a generalization of traditional first-order topological insulators so that for an n -dimensional system, $(n-m)$ -dimensional edge states with $m \geq 2$ emerge. To date, there have been extensive studies of HOTIs from various fields of physics [1–39] and several predicted topological phases have been experimentally observed [40–50]. Two typical HOTIs include two-dimensional (2D) quadrupole topological insulators with zero-energy corner-localized states characterized by a quantized quadrupole moment [3, 8] and three-dimensional (3D) second-order topological insulators with nonzero-energy chiral hinge states characterized by the Chern number of Wannier bands [11]. However, whether a system can host both zero-energy corner modes and nonzero-energy chiral modes is still elusive.

The Aubry-André-Harper (AAH) model [51, 52], a one-dimensional (1D) system with on-site cosinusoidal modulations, plays a crucial role in studying the Anderson localization and quasicrystals [53–58]. Recently, it has been found that such a model can also exhibit topological properties [59–68]. For instance, the model can be mapped to a 2D quantum Hall insulator that hosts nonzero energy topological edge modes characterized by the first Chern number [59–61]. This model has been further generalized to an off-diagonal AAH model with modulations in the hopping terms [62, 68], supporting topologically protected zero-energy modes. Such a model can support the coexistence of topological zero-energy and nonzero energy modes [62]. It is natural to ask whether we can construct a higher-order topological system based on the 1D AAH model so that the coexistence of these two topological phenomena can be observed.

Another interesting phenomenon concerns the existence of localized states in the continuous bulk spectrum

of a system, which are known as bound states in the continuum (BICs). BICs have been widely investigated in a wide range of physical systems, such as optical systems [69–72], plasmonic-photonic systems [73–78], acoustics [79–84], quantum dots [85–89] and water waves [90–95]. Recently, it has been shown that BICs can exist in topological systems [96–99]. Similar to other classical systems, an electric network system has recently been proven to be a powerful platform to simulate topological phenomena [42, 68, 100–102]. However, whether such systems can support BICs has not yet been explored. We will report a proposal with an electric circuit to realize a higher-order AAH model supporting BICs.

In this Rapid Communication, we address these important questions by constructing a 2D AAH lattice model based on 1D commensurate off-diagonal AAH models. We find that (i) zero-energy and nonzero-energy corner-localized states can coexist in the system. The former is protected by a quantized quadrupole moment and the latter is protected by the Chern number of the boundary bands as well as the Chern number of the Wannier bands. More interestingly, these nonzero-energy corner modes can exist in a continuous bulk spectrum forming bound states in the continuum. (ii) After transforming the system into a 3D lattice model, the system becomes a topological semimetal at half filling with gapless points located either on the surfaces or in the bulk. (iii) For the 3D system, besides the topological zero-energy modes localized at the hinges, the system also exhibits nonzero-energy chiral hinge modes arising from the existence of Chern bands on the surfaces. (iv) We finally propose an experimental scheme to simulate the 2D AAH model using electric circuits and demonstrate the existence of BICs in the form of voltage waves in the circuit.

Model Hamiltonian.— We start by considering the fol-

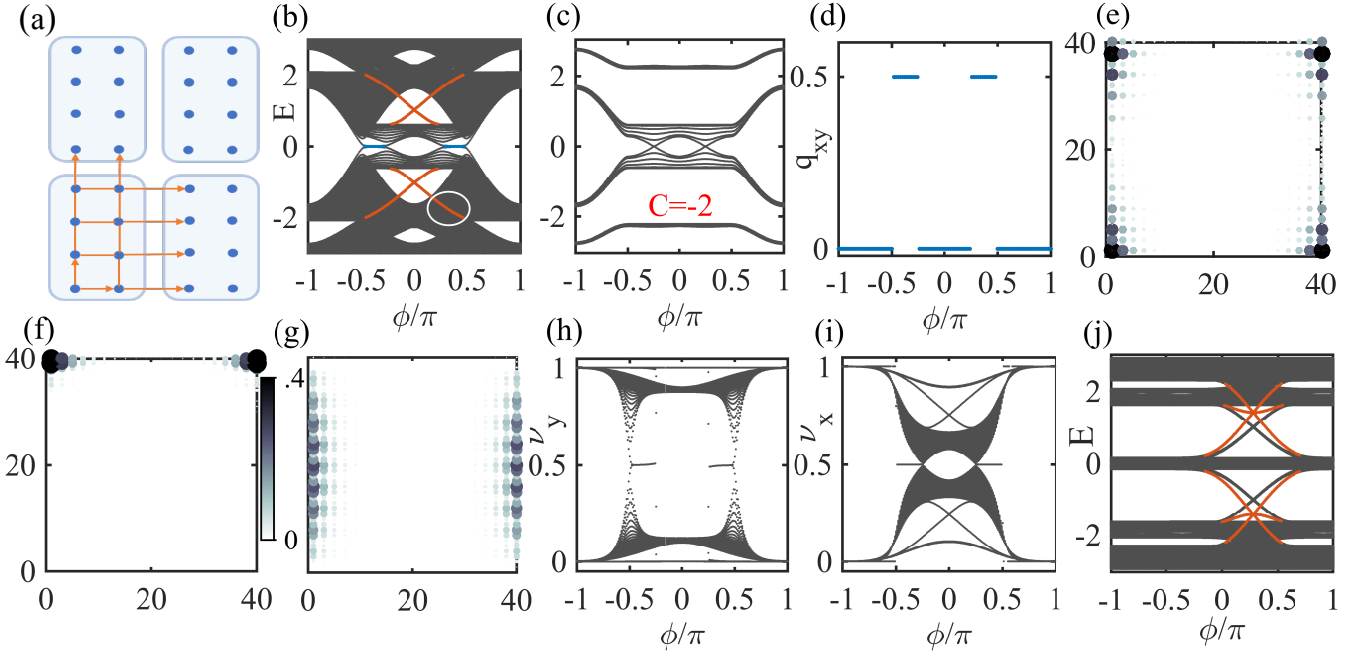


FIG. 1. (Color online) (a) Schematics of the tunneling for the 2D AAH lattice model with $\alpha_x = 1/2$ and $\alpha_y = 1/4$. (b) The energy spectrum obtained under open boundary conditions along both x and y directions. The lattice size is 40×40 . The blue and red lines describe the zero-energy and nonzero energy topological corner modes, respectively. The nonzero-energy corner modes highlighted by the white circle exist in a continuous bulk band. (c) The boundary bands obtained under periodic (open) boundary conditions along y (x). The red number denotes the Chern number contributed by the boundary bands. (d) The quadrupole moment in units of e as a function of ϕ at half filling. (e)-(g) display the spatial distribution of the wave-function amplitude for a zero-energy corner mode, the nonzero-energy corner modes, and the states for the boundary bands at $\phi = 0.35\pi$, respectively. The Wannier spectra ν_y (h) and ν_x (i) are computed under open boundary conditions along x and y directions, respectively. The presence of edge states around $\nu_x = 0.5$ and $\nu_y = 0.5$ in the Wannier spectra shows the existence of quantized edge polarizations. The Wannier band ν_x (similarly for ν_y) refers to the eigenvalues $2\pi\nu_x$ of the Wannier Hamiltonian $H_{\mathcal{W}_x}$ defined as $\mathcal{W}_x \equiv e^{iH\mathcal{W}_x}$, where $\mathcal{W}_x = F_{x,k_x+(N_x-1)\delta k_x} \cdots F_{x,k_x}$ is the Wilson loop with $[F_{x,k_x}]^{mn} = \langle u_{k_x+\delta k_x}^m | u_{k_x}^n \rangle$ [3, 8] and $|u_{k_x}^n\rangle$ is the n th occupied eigenstate of our system and $\delta k_x = 2\pi/L_x$, with L_x being the number of unit cells along x . Here, $t = 1$, $\lambda_x = \lambda_y = 0.8$, $\alpha_x = 1/2$, and $\alpha_y = 1/4$. (j) shows the energy spectrum for the incommensurate case with $\alpha = (\sqrt{5} - 1)/2$, where only nonzero-energy topological corner modes exist.

lowing 2D lattice model [see Fig. 1(a) for a schematic],

$$H = \sum_{i,j} [t_{(i,j),(i+1,j)} \hat{c}_{i,j}^\dagger \hat{c}_{i+1,j} + t_{(i,j),(i,j+1)} \hat{c}_{i,j+1}^\dagger \hat{c}_{i,j} + H.c.], \quad (1)$$

where $c_{i,j}^\dagger$ ($c_{i,j}$) represents the creation (annihilation) operator for a spinless particle at site (i,j) . The hopping amplitudes along the x and y directions are respectively modulated as

$$t_{(i,j),(i+1,j)} = (-1)^j t_x [1 + \lambda_x \cos(2\pi\alpha_x i + \phi_x)],$$

$$t_{(i,j),(i,j+1)} = t_y [1 + \lambda_y \cos(2\pi\alpha_y j + \phi_y)],$$

where $\alpha_x = p_x/q_x$, $\alpha_y = p_y/q_y$ with p_x and q_x (p_y and q_y) being mutually prime positive integers, t_x (t_y) is the hopping strength between the nearest-neighboring lattice sites along the x (y) direction, and λ_x and λ_y are the amplitudes of the modulations whose periods are determined by α_x and α_y . Without loss of generality, we set $t_x = t_y = t$ and $\phi_x = \phi_y = \phi$. The 2D lattice is actually

composed by 1D commensurate off-diagonal AAH models. If $\alpha_x = \alpha_y = 1/2$, the system exhibits zero-energy corner modes with a quantized electric quadrupole moment, similar to the model in [3].

With periodic boundary conditions in both directions, we can write the Hamiltonian in Eq.(1) in the momentum space as [103]

$$H(k_x, k_y) = H_x(k_x) \otimes \Pi_y + I_x \otimes H_y(k_y), \quad (2)$$

where $H_i(k_i)$ ($i = x, y$) is the Hamiltonian of the 1D AAH model along the i direction with $k_i \in [0, 2\pi)$. Such a 1D Hamiltonian is a $q_i \times q_i$ matrix, which, when q_i is even, has chiral symmetry represented by a $q_i \times q_i$ diagonal matrix $\Pi_i = \text{diag}(1 \ -1 \ \cdots \ 1 \ -1)$, i.e., $\Pi_i H_i \Pi_i^\dagger = -H_i$. I_x is an identity matrix of size q_x . Clearly, the 2D Hamiltonian has chiral symmetry, $\Pi H \Pi^\dagger = -H$ with $\Pi = \Pi_x \otimes \Pi_y$. For the 1D AAH model with $q_i > 2$, we can obtain chiral edge modes by tuning the parameter ϕ , which leads to topological Chern bands. In the following, we will explore whether the 2D lattice composed of such

1D AAH models can give rise to new topological features.

Case $\alpha_x = 1/2$ and $\alpha_y = 1/4$.— We first consider the model with $\alpha_x = 1/2$ and $\alpha_y = 1/4$. Figure 1(b) shows the energy spectrum of the lattice model under open boundary conditions along both directions. For $\phi \in (-\frac{\pi}{2}, -\frac{\pi}{4})$ and $(\frac{\pi}{4}, \frac{\pi}{2})$, we can observe zero-energy modes in the gap marked by the blue lines. They are four-fold degenerate and localized at the four corners of the 2D lattice, as illustrated in Fig. 1(e). The topological zero-energy corner states signify the existence of quadrupole moments in the system. To prove this, we have numerically calculated the quadrupole moment of the model as a function of ϕ based on the following formula [104, 105]

$$q_{xy} = \frac{e}{2\pi} \text{Im} \log \det U, \quad (3)$$

where $U_{nm} = \langle u_n | e^{i2\pi xy / (L_x L_y)} | u_m \rangle$ with $|u_m\rangle$ being the m th occupied eigenstate and L_x (L_y) being the length of our system in the x (y) direction relative to the unit cells. We perform our calculation under periodic boundary conditions. Due to the chiral symmetry, the quadrupole moments are quantized to 0 or $e/2$ modulo one.

In Fig. 1(d), we present the quadrupole moment with respect to ϕ , showing that the quadrupole moments are equal to $e/2$ in the parameter regimes where the zero-energy corner states emerge. This implies that the zero-energy states are characterized by the quantized quadrupole moment. We can also understand the presence of zero-energy corner states from the topology of the 1D AAH model [103]. Consider a system with a cylinder geometry with open boundaries along x and periodic boundaries along y . If H_x is topologically nontrivial, there are two zero-energy edge states for H_x denoted as $|u_{xL}\rangle$ and $|u_{xR}\rangle$ localized at the left and right edge, respectively. Clearly, the effective Hamiltonian of our 2D system at one edge around zero energy is $H_y(k_y)$, resulting in two zero-energy corner states if H_y is topologically nontrivial and we impose open boundary conditions along y . Specifically, a state localized at the top left corner can be written as $|u_{xL}\rangle \otimes |u_{yT}\rangle$, where $|u_{yT}\rangle$ is the zero-energy edge state of H_y localized at the top edge. Since H_x and H_y respect the chiral symmetry, their zero-energy edge states can be characterized by the winding number W_x and W_y , respectively. As a result, their product $W = W_x W_y$ gives another diagnosis of the topological property for the 2D system, apart from the quadrupole moment. Since the zero-energy state emerges for $H_x(k_x)$ with $\alpha_x = 1/2$ when $\phi \in (-\frac{\pi}{2}, \frac{\pi}{2})$ and for $H_y(k_y)$ with $\alpha_y = 1/4$ when $\phi \in (-\frac{\pi}{2}, -\frac{\pi}{4})$ and $(\frac{\pi}{4}, \frac{\pi}{2})$, the intersection of ϕ where both zero-energy states exist corresponds to the parameter region observed in Fig. 1(d). Due to the chiral symmetry, the zero-energy edge modes of the 1D AAH model are characterized by winding numbers. By combining the two winding numbers along the x and y directions, the zero-energy corner modes can be characterized [103], which is consistent with the quadrupole

moment results here.

It is known that the quadrupole moment can change due to the bulk or edge energy gap closure [3, 39]. In our system, at $\phi = \pm\pi/2$, the change arises from the y -normal edge energy gap closure, and at $\phi = \pm\pi/4$, from the x -normal edge energy gap closure. The former (latter) gap closure also leads to the gap closure for the Wannier band ν_y (ν_x) [see Figs. 1(h) and 1(i), respectively]. As a consequence, the edge polarizations along both directions $p_x^{\text{edge}} = p_y^{\text{edge}} = e/2$ in the topological region with quadrupole moments. In addition, fractional corner charges appear as $Q^{\text{corner}} = \pm e/2$ at half filling since there are four zero-energy corner modes. This shows that the basic relation $Q^{\text{corner}} = (p_y^{\text{edge}} + p_x^{\text{edge}} - q_{xy}) \text{mod}(1)$ is respected and thus it is a type-I quadrupole topological insulator [39].

Apart from the zero-energy corner modes, we also observe nonzero-energy topological corner modes in the energy spectrum, as shown by the red lines in Fig. 1(b). If ϕ is viewed as the momentum along z , these modes are chiral and we thus refer to these modes as chiral modes. In the following, we will show that these modes arise from a surface Chern insulator. By calculating the energy spectrum of the system with periodic and open boundaries along y and x , respectively, we extract the boundary bands [shown in Fig. 1(c)] based on their localization property [106]. These bands are twofold degenerate with the states localized at either the right or left edge. The nonzero-energy topological modes connecting these boundary bands are characterized by the Chern number defined in the (k_y, ϕ) space as

$$C_n = \frac{1}{2\pi} \int_0^{2\pi} d\phi \int_0^{2\pi} dk_y \Omega_n(k_y, \phi), \quad (4)$$

where $\Omega_n = i(\langle \partial_{k_y} \Psi_n | \partial_\phi \Psi_n \rangle - k_y \leftrightarrow \phi)$ with $|\Psi_n\rangle$ being the states in the boundary band extracted from the energy spectrum for a system with periodic boundaries along y . We find $C = -2$ for the lowest bands in Fig. 1(c) due to the degeneracy, with each boundary band localized at one of the two edges contributing a Chern number of -1 .

If we take ϕ as the momentum k_z along the z direction, the 2D AAH model can be transformed into a 3D model (the corresponding tight-binding Hamiltonian can be found in the Supplemental Material). This 3D model describes a 3D topological semimetal at half filling, where gapless points exist on both x -normal and y -normal surfaces [see Figs. 1(b) and 1(c)]. The zero-energy corner modes then contribute to the zero-energy hinge modes in the semimetal. In addition, the system exhibits a surface Chern band localized on the x -normal surfaces, leading to the chiral hinge modes.

The nonzero-energy corner modes (or chiral hinge modes in 3D) are in fact rooted in the topological properties of bulk energy bands. To illustrate this, we calculate the Chern number of the Wannier bands, which are

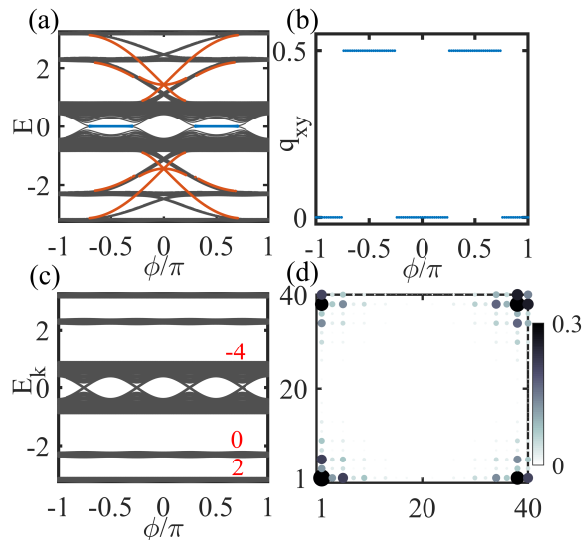


FIG. 2. (Color online) (a) The energy spectrum obtained under open boundary conditions along both x and y directions. The lattice size is 40×40 . The red lines describe the chiral corner modes with respect to ϕ inside the gap. (b) The quadrupole moments in units of e as a function of ϕ . (c) The energy spectrum obtained under periodic boundary conditions along both directions. The red numbers denote the Chern number calculated in the (k_y, ϕ) or (k_x, ϕ) space using the states of the corresponding bands for each k_x or k_y . (d) The spatial profile of the zero-energy corner modes. Here, $t = 1$, $\lambda_x = \lambda_y = 0.8$, and $\alpha_x = \alpha_y = 1/4$.

obtained based on the lowest two degenerate occupied bands [106], and find that the Chern number is equal to one, which is consistent with the existence of one chiral mode at each corner. Since this topological invariant is calculated using the wave functions under periodic boundary conditions, it shows that the nonzero-energy topological modes arise from the topological properties of bulk states.

Another important observation of this model is that such nonzero energy corner modes can exist in the continuous bulk spectrum as indicated by the white circle in Fig. 1(b). These corner states lying in the continuum of the extended bulk states form the BICs. Such BICs also survive in the incommensurate lattice where the chiral symmetry is broken, as shown in Fig. 1(j). Therefore, our 2D AAH model also provides a platform for studying the BICs in higher-order topological systems.

Case $\alpha_x = \alpha_y = 1/4$.— We now investigate the case where the modulations have the same period in both directions, e.g., $\alpha_x = \alpha_y = 1/4$. In Fig. 2(a), we display the energy spectrum for a lattice under open boundary conditions along both directions. Again, the zero-energy modes show up for $\phi \in (-\frac{3\pi}{4}, -\frac{\pi}{4})$ and $(\frac{\pi}{4}, \frac{3\pi}{4})$, which coincide with the regime for the emergence of zero-energy edge modes in the 1D AAH model. The zero-energy modes are fourfold degenerate corresponding to the cor-

ner states shown in Fig. 2(d). Similar to the preceding case, the zero-energy corner modes are characterized by the quantized quadrupole moment, as shown in Fig. 2(b). In this case, the quadrupole moment arises from the bulk energy gap closure [see Fig. 2(c)], instead of the edge gap closure. These topological quadrupole insulators are also type-I since $p_x^{\text{edge}} = p_y^{\text{edge}} = e/2$.

In addition to the zero-energy corner modes, we also find nonzero energy chiral modes inside the gaps of the energy spectrum. One group of chiral modes in the bulk gaps are boundary bands with states localized at the 1D edges. They are characterized by the Chern number computed in the (k_y, ϕ) or (k_x, ϕ) space using Eq.(4) for each k_x or k_y , as denoted by the red numbers in Fig. 2(c). The other chiral modes, marked by the red lines in Fig. 2(a), connect different boundary bands and are localized at the corners. Compared to the preceding case, the Chern number of the boundary states is not well defined since these bands are chiral and not well separated. Similarly, we can transform the 2D model into a 3D model with gapless points in the bulk [see Fig. 2(c)], where the zero-energy and nonzero energy corner states become the zero-energy and nonzero-energy chiral modes localized at the hinges along z .

Experimental realization.— Here, we propose an experimental scheme to realize the 2D AAH model with electric circuits. In fact, the quadrupole topological insulators with zero-energy corner modes have been experimentally observed in electric circuits [42]. We apply a similar method to construct an electric network to simulate the 2D AAH model using the Laplacian of the circuit (see the details in the Supplemental Material). The quadrupole moment can be measured by probing the single-point impedances of the circuit [39] and the existence of the corner modes can be detected by measuring the resonance of two-point impedances near the corners [39, 42, 68]. In addition, we can use the electric network to simulate the dynamics of the Schrödinger equation. In this case, the dynamics is governed by a circuit Hamiltonian (usually different from the Laplacian) which can also support the zero-energy corner modes and nonzero-energy chiral modes. Remarkably, we find the presence of chiral corner modes in the continuous bulk spectrum, indicating the existence of BICs in the electric circuit. Besides the electric circuit, our model can also be realized in other systems, such as solid-state materials, cold atoms, and photonic and phononic crystals.

In summary, we have constructed a generalized 2D AAH model that supports the coexistence of zero-energy corner modes characterized by the quantized quadrupole moment and nonzero-energy corner modes characterized by the Chern number of the boundary bands and the Chern number of the Wannier bands. This model actually describes a 3D higher-order topological semimetal with the coexistence of zero-energy hinge modes and nonzero-energy chiral modes contributed by a Chern

band on the surfaces. In addition, we also find that nonzero-energy chiral modes can form the bound states in the continuum. Finally, we propose a practical scheme to realize the 2D AAH model in electric circuits. Our model provides another platform for realizing and detecting the exotic properties of higher-order topological insulators and semimetals.

This work is supported by the start-up fund from Tsinghua University, the National Thousand-Young-Talents Program and the National Natural Science Foundation of China (11974201).

Note added. Recently, we became aware of a related work on higher-order topological insulators [107].

SUPPLEMENTAL MATERIAL

In the supplementary material, we will show how the boundary bands are extracted, provide the 3D tight-binding Hamiltonian in real space obtained by transforming the 2D AAH model, present the method to evaluate the Chern number of Wannier bands and introduce the detailed experimental scheme for realizing the 2D AAH model in electric circuits.

S1. THE BOUNDARY CHERN BAND

To show the existence of a Chern band at the edge, we plot the energy spectrum of the 2D AAH model in a cylinder geometry with open and periodic boundaries along x and y , respectively, in Fig. S1(a). To distinguish the bulk and edge modes, we calculate the inverse participation ratio (IPR) for each eigenstates $|\Psi_n\rangle$ with the corresponding eigenenergies E_n , which is defined as

$$\text{IPR} = \sum_j \frac{|\Psi_{n,j}|^4}{(\langle \Psi_n | \Psi_n \rangle)^2}, \quad (\text{S1})$$

with $\Psi_{n,j}$ being the j th component of the eigenstate vector. The IPR values of the edge modes are much larger than the bulk states, as shown in Fig. S1(a). We therefore can extract the boundary bands based on the IPR values. Specifically, we take $\phi = 0$ and pick out the eigenstates with IPR values larger than a threshold value, say, for example, 0.025, and get the indices of these states. The boundary bands are composed of the states with the same indices at each ϕ value [Fig. S1(b)]. After that, we calculate the Chern number of these boundary bands as presented in the main text.

S2. THE TIGHT-BINDING MODEL IN 3D

If we regard the parameter ϕ as the momentum k_z along z , we obtain a Hamiltonian describing a 3D system. By performing the Fourier transformation, we obtain the following tight-binding Hamiltonian in real space

$$\begin{aligned} H_{3D} = \sum_{j_x, j_y, j_z} & \left[t_x (-1)^{j_y} \hat{c}_{j_x, j_y, j_z}^\dagger \hat{c}_{j_x+1, j_y, j_z} + t_y \hat{c}_{j_x, j_y+1, j_z}^\dagger \hat{c}_{j_x, j_y, j_z} \right. \\ & + \frac{t_x \lambda_x}{2} (-1)^{j_y} e^{i2\pi\alpha_x j_x} (\hat{c}_{j_x, j_y, j_z}^\dagger \hat{c}_{j_x+1, j_y, j_z+1} + \hat{c}_{j_x+1, j_y, j_z}^\dagger \hat{c}_{j_x, j_y, j_z+1}) \\ & \left. + \frac{t_y \lambda_y}{2} e^{i2\pi\alpha_y j_y} (\hat{c}_{j_x, j_y+1, j_z}^\dagger \hat{c}_{j_x, j_y, j_z+1} + \hat{c}_{j_x, j_y, j_z}^\dagger \hat{c}_{j_x, j_y+1, j_z+1}) + H.c. \right]. \quad (\text{S2}) \end{aligned}$$

S3. THE CHERN NUMBER OF THE WANNIER BANDS

In the case of $(\alpha_x, \alpha_y) = (1/2, 1/4)$, we first calculate the Wilson loop matrix along the x direction for the lowest doubly degenerate bands (separated from the other bands) [3, 8],

$$\mathcal{W}_{x, \mathbf{k}} = F_{x, \mathbf{k} + (N_x - 1)\delta\mathbf{k}_x} \cdots F_{x, \mathbf{k} + \delta\mathbf{k}_x} F_{x, \mathbf{k}}, \quad (\text{S3})$$

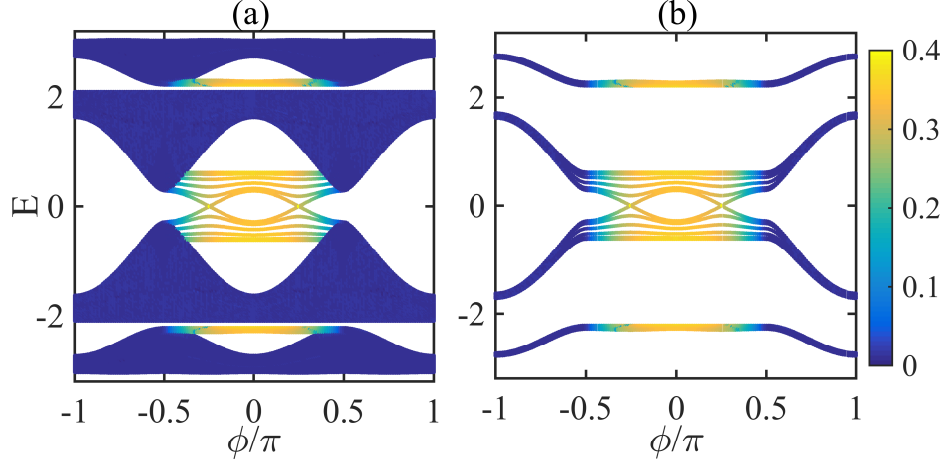


FIG. S1. (Color online) (a) The energy spectrum of the 2D AAH model with open boundaries along x and periodic boundaries along y . (b) The boundary bands extracted from the energy spectrum in (a). The color bar indicates the IPR value of the corresponding eigenstates. Here $t = 1$, $\lambda_x = \lambda_y = 0.8$, $\alpha_x = 1/2$ and $\alpha_y = 1/4$. The lattice size is 40×40 .

where $[F_{x,\mathbf{k}}]^{mn} = \langle u_{\mathbf{k}+\delta\mathbf{k}_x}^m | u_{\mathbf{k}}^n \rangle$ and $\delta\mathbf{k}_x = (2\pi/N_x, 0)$ with $|u_{\mathbf{k}}^n\rangle$ being the occupied eigenstate. The Wannier Hamiltonian $H_{\mathcal{W}_{x,\mathbf{k}}}$ is defined as

$$\mathcal{W}_{x,\mathbf{k}} = e^{iH_{\mathcal{W}_{x,\mathbf{k}}}}, \quad (\text{S4})$$

which is related to the boundary bands with the edge perpendicular to the x direction [108].

Using the spectral decomposition, the Wilson loop matrix $\mathcal{W}_{x,(\mathbf{k},\phi)}$ can be written as

$$\mathcal{W}_{x,(\mathbf{k},\phi)} = \sum_{j=\pm} e^{2\pi i \nu_x^j(k_y, \phi)} |\nu_{x,(\mathbf{k},\phi)}^j\rangle \langle \nu_{x,(\mathbf{k},\phi)}^j|, \quad (\text{S5})$$

where $|\nu_{x,(\mathbf{k},\phi)}^j\rangle$ is the eigenvector of $\mathcal{W}_{x,(\mathbf{k},\phi)}$ with the corresponding eigenvalue of $e^{2\pi i \nu_x^j(k_y, \phi)}$. We refer to the eigenvalues of $\nu_x^j(k_y, \phi)$ as the Wannier bands. Since $e^{2\pi i \nu_x^j(k_y, \phi)}$ repeats over 1 for $\nu_x^j(k_y, \phi)$, we restrict them to $[0, 1)$. As shown in Fig. S2, there appear two Wannier bands that are gapped around $\nu_x = 0.5$, leading to two Wannier sectors denoted by ν_x^- for the band below the Wannier gap and ν_x^+ for the band above the Wannier gap.

Analogous to the Wannier-sector polarization [3, 8], we define the Wannier-sector Chern number using the Wannier basis [11]

$$C_{k_y, \phi}^{\nu_x^\pm} = \frac{1}{2\pi} \frac{1}{N_x} \sum_{k_x} \int_0^{2\pi} d\phi \int_0^{2\pi} dk_y \tilde{\Omega}_{k_x, (k_y, \phi)}^\pm, \quad (\text{S6})$$

where $\tilde{\Omega}_{k_x, (k_y, \phi)}^\pm = i(\langle \partial_{k_y} w_{x,(\mathbf{k},\phi)}^\pm | \partial_\phi w_{x,(\mathbf{k},\phi)}^\pm \rangle - k_y \leftrightarrow \phi)$ and

$$|w_{x,(\mathbf{k},\phi)}^\pm\rangle = \sum_{n=1,2} |u_{\mathbf{k}}^n\rangle [\nu_{x,(\mathbf{k},\phi)}^\pm]^n. \quad (\text{S7})$$

In the thermodynamic limit, the Chern number of the Wannier band is

$$C_{k_y, \phi}^{\nu_x^\pm} = \frac{1}{4\pi^2} \int_0^{2\pi} d\phi \int_{BZ} d^2\mathbf{k} \tilde{\Omega}_{k_x, (k_y, \phi)}^\pm. \quad (\text{S8})$$

For the lowest two occupied bands, we find that the Chern numbers of Wannier sectors are $C_{k_y, \phi}^{\nu_x^+} = C_{k_y, \phi}^{\nu_x^-} = 1$, which characterize the chiral corner modes. This topological invariant is equivalent to the Chern number of boundary bands defined in the main text.

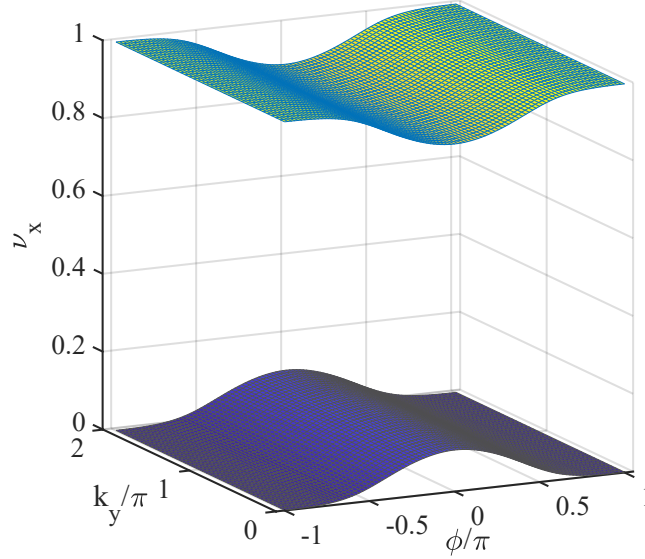


FIG. S2. (Color online) The Wannier bands for the system with $\alpha_x = 1/2$ and $\alpha_y = 1/4$ obtained by diagonalizing the Wilson loop matrix [see the formula (S3)]. Here $t = 1$ and $\lambda_x = \lambda_y = 0.8$.

S4. EXPERIMENTAL REALIZATION IN ELECTRIC CIRCUIT

In this section, we present the experimental scheme in detail for realizing the 2D AAH model in electric circuit. Fig. S3(a) illustrates an electric network composed of capacitors and inductors. This network can be used to simulate our 2D Hamiltonian with lattice sites described by the circuit nodes indicated by red indices. If we denote the input currents and voltages at each node as a N -component column vector \mathbf{I} and \mathbf{V} , respectively, it is straightforward to obtain a relation expressed as $\mathbf{I} = \mathbf{J}\mathbf{V}$, according to the Kirchhoff's law. Here \mathbf{J} is the Laplacian of the circuit. Our Hamiltonian can be simulated by the Laplacian through $\mathbf{J} = i\mathbf{H}$. Specifically, the connection between the neighboring nodes through inductors or capacitors can imitate the hopping between neighboring lattice sites. If the hopping is negative (positive), the two nodes are connected by an inductor (a capacitor). For a specific node (m, n) , we set the impedance of the device as $1/Z_{xm} = it[1 + \lambda_x \cos(2\pi\alpha_x m + \phi_x)]$ and $1/Z_{yn} = it[1 + \lambda_y \cos(2\pi\alpha_y n + \phi_y)]$ (here i refers to the imaginary unit). In addition, we need to eliminate the diagonal terms by grounding every node through a capacitor (inductor) with appropriate impedance $1/Z'_{m,n} = -(1/Z_{xm} + 1/Z_{x,m-1} + 1/Z_{yn} + 1/Z_{y,n-1})$.

To study the bound states in the continuum (BICs) which are stable against scattering to the bulk states, we need to investigate the dynamics in electric circuits. In fact, the dynamics of a wave packet in a Chern insulator [109] and the dynamics of a hinge soliton in a 3D higher-order topological insulator [110] have been studied in electric circuits. The time evolution of the circuit is governed by [109, 110]

$$\frac{d}{dt}\mathbf{I}(t) = C\frac{d^2}{dt^2}\mathbf{V}(t) + \Sigma\frac{d}{dt}\mathbf{V}(t) + L\mathbf{V}(t), \quad (\text{S9})$$

where C , Σ , and L are real-valued matrices for capacitance, conductance, and inductance, respectively. The circuit Laplacian for alternating currents with frequency ω is given by

$$J(\omega) = i\omega C + \Sigma + \frac{1}{i\omega}L. \quad (\text{S10})$$

If there are no input currents ($\mathbf{I}(t) = 0$), the equation of motion of the circuit can be reduced to a first-order differential equation which is similar to the Schrödinger equation,

$$-i\frac{d}{dt}\psi(t) = H_c\psi(t), \quad (\text{S11})$$

where $\psi(t) = (\frac{d}{dt}\mathbf{V}(t), \mathbf{V}(t))^T$, and the circuit Hamiltonian is

$$H_c = i\begin{pmatrix} C^{-1}\Sigma & C^{-1}L \\ -\mathbf{1} & 0 \end{pmatrix}. \quad (\text{S12})$$

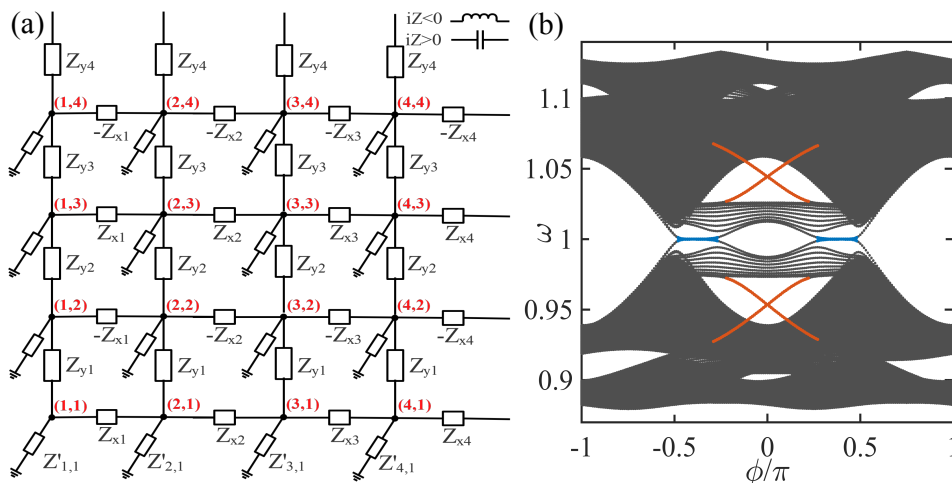


FIG. S3. (Color online) (a) The electric network for realizing the 2D AAH model. The red numbers in brackets label the indices of nodes corresponding to the lattice sites. The hopping between the neighboring lattice sites are simulated by the impedance of the electric device connecting the nodes. If the hopping amplitude is positive (negative), then Z is implemented by a capacitor (an inductor). Every node is grounded through a capacitor or an inductor to eliminate the diagonal terms. (b) The frequency spectrum ω of the circuit with respect to ϕ for the 2D AAH model with $\alpha_x = 1/2$ and $\alpha_y = 1/4$ in a geometry with open boundaries in all directions. The unit of ω is ω_0 .

The time evolution of an eigenstate of H_c is given by $\psi_n(t) = e^{i\omega_n t} \phi_n$, where ϕ_n is an eigenvector of H_c with the eigenfrequency ω_n ($n = 1, \dots, 2N$). It can be shown that the eigenfrequencies of H_c occur in real-valued pairs ($\omega_n, -\omega_n$) if the Laplacian matrix $J(\omega)$ satisfies $J(\omega) = -J(\omega)^\dagger$ for any real frequencies ω [109]. These eigenfrequencies $\{\omega_n\}$ of the circuit Hamiltonian H_c are also associated with the admittance eigenvalues $j(\omega)$ of the Laplacian $J(\omega)$ through $j(\omega_n) = 0$. Due to this intimate connection, the circuit Hamiltonian H_c owns similar band structures to those of the circuit Laplacian J [109]. For instance, if there exist four zero-energy corner modes in the eigenvalues of $J(\omega_0) = i\omega_0 H(\omega_0)$, i.e., $j_n(\omega_0) = 0$ with $n = 1, 2, 3, 4$, associated with the corresponding eigenvectors V_n , H_c also has four-fold degenerate frequency modes $(i\omega_0 V_n \ V_n)^T$ corresponding to the frequency ω_0 .

In Fig. S3(b), we plot the eigenfrequencies ω of H_c as a function of ϕ for the case with $\alpha_x = 1/2$ and $\alpha_y = 1/4$ in a geometry with open boundaries along both x and y directions. As expected, the frequency bands $\omega(\phi)$ exhibit four-fold degenerate corner modes with the eigenfrequency equal to the resonance frequency ω_0 , as shown by the blue lines in the figure. We also find chiral modes (red lines) localized at the corners as well, which is similar to the energy spectrum of the Hamiltonian H . It is interesting to see that parts of the chiral corner modes lie in the continuous bulk spectrum, forming BICs.

* These authors contributed equally to this work.

† yongxuphy@tsinghua.edu.cn

-
- [1] M. Sitte, A. Rosch, E. Altman, and L. Fritz, Phys. Rev. Lett. **108**, 126807 (2012).
- [2] F. Zhang, C. L. Kane, and E. J. Mele, Phys. Rev. Lett. **110**, 046404 (2013).
- [3] W. A. Benalcazar, B. A. Bernevig, and T. L. Hughes, Science **357**, 61 (2017).
- [4] R.-J. Slager, L. Rademaker, J. Zaanen, and L. Balents, Phys. Rev. B **92**, 085126 (2015).
- [5] J. Langbehn, Y. Peng, L. Trifunovic, F. von Oppen, and P.W. Brouwer, Phys. Rev. Lett. **119**, 246401 (2017).
- [6] Z. Song, Z. Fang, and C. Fang, Phys. Rev. Lett. **119**, 246402 (2017).
- [7] Y. Peng, Y. Bao, and F. von Oppen, Phys. Rev. B **95**, 235143 (2017).
- [8] W. A. Benalcazar, B. A. Bernevig, and T. L. Hughes, Phys. Rev. B **96**, 245115 (2017).
- [9] C. Fang and L. Fu, Sci. Adv. **5**, eaat2374 (2019).
- [10] Y. Xu, R. Xue, and S. Wan, [arXiv:1711.09202](https://arxiv.org/abs/1711.09202).
- [11] F. Schindler, A.M. Cook, M. G. Vergniory, Z. Wang, S. S. P. Parkin, B. A. Bernevig, and T. Neupert, Sci. Adv. **4**, eaat0346 (2018).
- [12] M. Ezawa, Phys. Rev. Lett. **120**, 026801 (2018).
- [13] Z. Yan, F. Song, and Z. Wang, Phys. Rev. Lett. **121**, 096803 (2018).
- [14] Q. Wang, C.-C. Liu, Y.-M. Lu, and F. Zhang, Phys. Rev. Lett. **121**, 186801 (2018).
- [15] H. Shapourian, Y. Wang, and S. Ryu, Phys. Rev. B **97**, 094508 (2018).
- [16] M. Geier, L. Trifunovic, M. Hoskam, and P.W. Brouwer, Phys. Rev. B **97**, 205135 (2018).
- [17] G. van Miert and C. Ortix, Phys. Rev. B **98**, 081110(R) (2018).

- [18] Y. Wang, M. Lin, and T. L. Hughes, *Phys. Rev. B* **98**, 165144 (2018).
- [19] S. Franca, J. van den Brink, and I. C. Fulga, *Phys. Rev. B* **98**, 201114(R) (2018).
- [20] A. Matsugatani and H. Watanabe, *Phys. Rev. B* **98**, 205129 (2018).
- [21] Y. You, T. Devakul, F. J. Burnell, and T. Neupert, *Phys. Rev. B* **98**, 235102 (2018).
- [22] M. Lin and T. L. Hughes, *Phys. Rev. B* **98**, 241103(R) (2018).
- [23] T. Liu, J. J. He, and F. Nori, *Phys. Rev. B* **98**, 245413 (2018).
- [24] B. Huang and W. V. Liu, *Phys. Rev. Lett.* **124**, 216601 (2020).
- [25] L. Trifunovic, and P. W. Brouwer, *Phys. Rev. X* **9**, 011012 (2019).
- [26] F. Liu, H.-Y. Deng, and K. Wakabayashi, *Phys. Rev. Lett.* **122**, 086804 (2019).
- [27] X.-H. Pan, K.-J. Yang, L. Chen, G. Xu, C.-X. Liu, and X. Liu, *Phys. Rev. Lett.* **123**, 156801 (2019).
- [28] R.-X. Zhang, W. S. Cole, X. Wu, and S. Das Sarma, *Phys. Rev. Lett.* **123**, 167001 (2019).
- [29] Z. Yan, *Phys. Rev. Lett.* **123**, 177001 (2019).
- [30] Z. Wang, B. J. Wieder, J. Li, B. Yan, and B. A. Bernevig, *Phys. Rev. Lett.* **123**, 186401 (2019).
- [31] M. J. Park, Y. Kim, G. Y. Cho, and S. B. Lee, *Phys. Rev. Lett.* **123**, 216803 (2019)
- [32] D. Călugăru, V. Juričić, and B. Roy, *Phys. Rev. B* **99**, 041301(R) (2019).
- [33] O. Dubinkin and T. L. Hughes, *Phys. Rev. B* **99**, 235132 (2019).
- [34] R. Chen, C.-Z. Chen, J.-H. Gao, B. Zhou, and D.-H. Xu, *Phys. Rev. Lett.* **124**, 036803 (2020).
- [35] Y.-Z. Chou, Y. Fu, J. H. Wilson, E. J. König, and J. H. Pixley, [arXiv:1908.09837](https://arxiv.org/abs/1908.09837).
- [36] E. Khalaf, W. A. Benalcazar, T. L. Hughes, and R. Queiroz, [arXiv:1908.00011](https://arxiv.org/abs/1908.00011).
- [37] R.-X. Zhang, Y.-T. Hsu, and S. Das Sarma, [arXiv:1909.07980](https://arxiv.org/abs/1909.07980).
- [38] B. J. Wieder, Z. Wang, J. Cano, X. Dai, L. M. Schoop, B. Bradlyn, and B. A. Bernevig, *Nat. Commun.* **11**, 627 (2020).
- [39] Y.-B. Yang, K. Li, L.-M. Duan, and Y. Xu, [arXiv:1910.04151](https://arxiv.org/abs/1910.04151).
- [40] M. Serra-Garcia, V. Peri, R. Süsstrunk, O. R. Bilal, T. Larsen, L. G. Villanueva, and S. D. Huber, *Nature (London)*, **555**, 342 (2018).
- [41] C. W. Peterson, W. A. Benalcazar, T. L. Hughes, and G. Bahl, *Nature (London)*, **555**, 346 (2018).
- [42] S. Imhof, C. Berger, F. Bayer, J. Brehm, L. W. Molenkamp, T. Kiessling, F. Schindler, C. H. Lee, M. Greiter, T. Neupert and R. Thomale, *Nat. Phys.* **14**, 925 (2018).
- [43] X. Zhang, H.-X. Wang, Z.-K. Lin, Y. Tian, B. Xie, M.-H. Lu, Y.-F. Chen, and J.-H. Jiang, *Nat. Phys.* **15**, 582 (2018).
- [44] F. Schindler, Z. Wang, M. G. Vergniory, A.M. Cook, A. Murani, S. Sengupta, A. Y. Kasumov, R. Deblock, S. Jeon, I. Drozdov, H. Bouchiat, S. Guéron, A. Yazdani, B. A. Bernevig, and T. Neupert, *Nat. Phys.* **14**, 918 (2018).
- [45] H. Xue, Y. Yang, F. Gao, Y. Chong, and B. Zhang, *Nat. Mater.* **18**, 108 (2019).
- [46] X. Ni, M. Weiner, A. Alù, and A. B. Khanikaev, *Nat. Mater.* **18**, 113 (2019).
- [47] S. Mittal, V. Vikram Orre, G. Zhu, M. A. Gorlach, A. Poddubny, and M. Hafezi, *Nat. Photonics* **13**, 692 (2019).
- [48] H. Xue, Y. Yang, G. Liu, F. Gao, Y. Chong, and B. Zhang, *Phys. Rev. Lett.* **122**, 244301 (2019).
- [49] J. Bao, D. Zou, W. Zhang, W. He, H. Sun, X. Zhang, *Phys. Rev. B* **100**, 201406(R) (2019).
- [50] X. Ni, M. Li, M. Weiner, A. Alù, and A. B. Khanikaev, *Nat. Commun.* **11**, 2108 (2020).
- [51] S. Aubry and G. André, *Ann. Isr. Phys. Soc.* **3**, 133 (1980).
- [52] P. G. Harper, *Proc. Phys. Soc. London, Sect. A* **68**, 874 (1955).
- [53] S. Ostlund, R. Pandit, D. Rand, H. J. Schellnhuber, and E. D. Siggia, *Phys. Rev. Lett.* **50**, 1873 (1983).
- [54] M. Kohmoto, *Phys. Rev. Lett.* **51**, 1198 (1983).
- [55] S. Das Sarma, S. He, and X. C. Xie, *Phys. Rev. Lett.* **61**, 2144 (1988).
- [56] S. Das Sarma, S. He, and X. C. Xie, *Phys. Rev. B* **41**, 5544 (1990).
- [57] J. Biddle, B. Wang, D. J. Priour, Jr., and S. Das Sarma, *Phys. Rev. A* **80**, 021603(R) (2009).
- [58] J. Biddle and S. Das Sarma, *Phys. Rev. Lett.* **104**, 070601 (2010).
- [59] L.-J. Lang, X. Cai, and S. Chen, *Phys. Rev. Lett.* **108**, 220401 (2012).
- [60] Y. E. Kraus, Y. Lahini, Z. Ringel, M. Verbin, and O. Zilberberg, *Phys. Rev. Lett.* **109**, 106402 (2012).
- [61] Y. E. Kraus and O. Zilberberg, *Phys. Rev. Lett.* **109**, 116404 (2012).
- [62] S. Ganeshan, K. Sun, and S. Das Sarma, *Phys. Rev. Lett.* **110**, 180403 (2013).
- [63] X. Cai, L.-J. Lang, S. Chen, and Y. Wang, *Phys. Rev. Lett.* **110**, 176403 (2013).
- [64] F. Liu, S. Ghosh, and Y. D. Chong, *Phys. Rev. B* **91**, 014108 (2015).
- [65] J. Wang, X.-J. Liu, G. Xianlong, and H. Hu, *Phys. Rev. B* **93**, 104504 (2016).
- [66] Q.-B. Zeng, S. Chen, and R. Lü, *Phys. Rev. B* **94**, 125408 (2016).
- [67] C. M. Dai, W. Wang, and X. X. Yi, *Phys. Rev. A* **98**, 013635 (2018).
- [68] Q.-B. Zeng, Y.-B. Yang, and Y. Xu, *Phys. Rev. B* **101**, 020201(R) (2020).
- [69] S. Longhi, *Phys. Rev. A* **78**, 013815 (2008).
- [70] S. Longhi, *Phys. Rev. A* **79**, 023811 (2009).
- [71] F. Dreisow, A. Szameit, M. Heinrich, R. Keil, S. Nolte, A. Tünnermann, and S. Longhi, *Opt. Lett.* **34**, 2405 (2009).
- [72] Y. Plotnik, O. Peleg, F. Dreisow, M. Heinrich, S. Nolte, A. Szameit, and M. Segev, *Phys. Rev. Lett.* **107**, 183901 (2011).
- [73] P. Paddon and Jeff F. Young, *Phys. Rev. B* **61**, 2090 (2000).
- [74] V. Pacradouni, W. J. Mandeville, A. R. Cowan, P. Paddon, Jeff F. Young, and S. R. Johnson, *Phys. Rev. B* **62**, 4204 (2000).
- [75] T. Ochiai and K. Sakoda, *Phys. Rev. B* **63**, 125107 (2001).
- [76] S. Fan and J. D. Joannopoulos, *Phys. Rev. B* **65**, 235112 (2002).

- [77] C. W. Hsu, B. Zhen, J. Lee, S.-L. Chua, S. G. Johnson, J. D. Joannopoulos, and M. Soljacic, *Nature (London)* **499**, 188 (2013).
- [78] B. Zhen, C. W. Hsu, L. Lu, A. D. Stone, and M. Soljacic, *Phys. Rev. Lett.* **113**, 257401 (2014).
- [79] R. Parker, *J. Sound Vib.* **4**, 62 (1966).
- [80] R. Parker, *J. Sound Vib.* **5**, 330 (1967).
- [81] N. A. Cumpsty and D. S. Whitehead, *J. Sound Vib.* **18**, 353 (1971).
- [82] W. Koch, *J. Sound Vib.* **88**, 233 (1983).
- [83] R. Parker and S. A. T. Stoneman, *Proc. Inst. Mech. Eng., Part C* **203**, 9 (1989).
- [84] D. V. Evans, M. Levitin, and D. Vassiliev, *J. Fluid Mech* **261**, 21 (1994).
- [85] M. L. Ladron de Guevara, F. Claro, and P. A. Orellana, *Phys. Rev. B* **67**, 195335 (2003).
- [86] P. A. Orellana, M. L. Ladron de Guevara, and F. Claro, *Phys. Rev. B* **70**, 233315 (2004).
- [87] M. L. Ladron de Guevara and P. A. Orellana, *Phys. Rev. B* **73**, 205303 (2006).
- [88] K.-K. Voo and C. S. Chu, *Phys. Rev. B* **74**, 155306 (2006).
- [89] W. Gong, Y. Han, and G. Wei, *J. Phys. Condens. Matter* **21**, 175801 (2009).
- [90] F. Ursell, *Math. Proc. Cambridge Philos. Soc.* **47**, 347 (1951).
- [91] D. S. Jones, *Math. Proc. Cambridge Philos. Soc.* **49**, 668 (1953).
- [92] M. Callan, C. M. Linton, and D. V. Evans, *J. Fluid Mech.* **229**, 51 (1991).
- [93] C. H. Retzler, *Appl. Ocean Res.* **23**, 249 (2001).
- [94] P. J. Cobelli, V. Pagneux, A. Maurel, and P. Petitjeans, *Europhys. Lett.* **88**, 20006 (2009).
- [95] P. J. Cobelli, V. Pagneux, A. Maurel, and P. Petitjeans, *J. Fluid Mech.* **666**, 445 (2011).
- [96] B.-J. Yang, M. S. Bahramy, and N. Nagaosa, *Nat. Commun.* **4**, 1524 (2013).
- [97] Y. X. Xiao, G. Ma, Z. Q. Zhang, and C. T. Chan, *Phys. Rev. Lett.* **118**, 166803 (2017).
- [98] Z.-G. Chen, C. Xu, R. Al Jahdali, J. Mei, and Y. Wu, *Phys. Rev. B* **100**, 075120 (2019).
- [99] W. A. Benalcazar and A. Cerjan, *Phys. Rev. B* **101**, 161116 (2020).
- [100] C. H. Lee, S. Imhof, C. Berger, F. Bayer, J. Brehm, L. W. Molenkamp, T. Kiessling, and R. Thomale, *Commun. Phys.* **1**, 39 (2018).
- [101] Y. Lu, N. Jia, L. Su, C. Owens, G. Juzeliunas, D. I. Schuster, and J. Simon, *Phys. Rev. B* **99**, 020302(R) (2019).
- [102] Y.-B. Yang, T. Qin, D.-L. Deng, L.-M. Duan, and Y. Xu, *Phys. Rev. Lett.* **123**, 076401 (2019).
- [103] R. Okugawa, S. Hayashi, and T. Nakanishi, *Phys. Rev. B* **100**, 235302 (2019).
- [104] W. A. Wheeler, L. K. Wagner, and T. L. Hughes, *Phys. Rev. B* **100**, 245135 (2019).
- [105] B. Kang, K. Shiozaki, and G. Y. Cho, *Phys. Rev. B* **100**, 145134 (2019).
- [106] See Supplemental Material for a method to extract the boundary bands, a 3D tight-binding Hamiltonian in real space, a method to evaluate the Chern number of Wannier bands and an experimental scheme for realizing the 2D AAH model in electric circuits.
- [107] I. Petrides and O. Zilberberg, [arXiv:1911.08461](https://arxiv.org/abs/1911.08461) (2019).
- [108] L. Fidkowski, T. S. Jackson, and I. Klich, *Phys. Rev. Lett.* **107**, 036601 (2011).
- [109] H. Hofmann, T. Helbig, C.-H. Lee, M. Greiter, and R. Thomale, *Phys. Rev. Lett.* **122**, 247702 (2019).
- [110] Y.-L. Tao, N. Dai, Y.-B. Yang, Q.-B. Zeng, and Y. Xu, [arXiv:2005.04433](https://arxiv.org/abs/2005.04433).